Variational charge relaxation in ionic crystals: An efficient treatment of statics and dynamics

A. Chizmeshya
Idaho National Engineering Laboratory, EG&G Idaho Inc., P.O. Box 1625, Idaho Falls, Idaho 83415

Frank M. Zimmermann
Physics Department, Clark Hall, Cornell University, Ithaca, New York 14853

Randall A. LaViolette
Idaho National Engineering Laboratory, EG&G Idaho Inc., P.O. Box 1625, Idaho Falls, Idaho 83415

George H. Wolf
Department of Chemistry, Arizona State University, Tempe, Arizona 85287
(Received 24 January 1994; revised manuscript received 6 July 1994)

An *ab initio* variationally induced breathing (VIB) description of the energetics and dynamics of ionic crystals is developed within the spherical-ion-pair approximation and the Gordon-Kim ansatz. In the VIB method, the total crystal charge density is given by the overlap of Kohn-Sham ionic charge densities. Spherical charge deformation of the ions is accomplished by adding an effective many-body crystal site potential to the atomic potential used in the Kohn-Sham procedure. Parameters defining this effective site potential are treated variationally such that the total crystal electronic energy is a minimum for a given structural configuration. We have explored a number of forms of the effective potential, including Watson-sphere types where both the charge and radius of the sphere are variationally determined. In addition, we have investigated anion-cation charge transfer by incorporating an additional variational parameter. We also present a formulation of the lattice dynamics of ionic crystals based on the VIB prescription in which the electronic variational parameters are treated as dynamical variables within the adiabatic approximation. With the computed phonon density of states, the structural parameters of a crystal can then be determined at any temperature and pressure (or stress condition) by minimizing the quasiharmonic Gibbs free energy with respect to the structural parameters along the electronic adiabatic surface. The complete pressure- and temperature-dependent thermal and elastic properties of a crystal can also be determined. We have applied the VIB procedure to calculate the equations of state, elastic properties, phonon dispersion relations, and phase stability of the alkaline earth oxides (MgO, CaO, and SrO). The calculated properties are generally in quite good agreement with experiment. Spherical charge deformation within the ionic description is responsible for a considerable improvement over rigid-ion elastic constants and bulk moduli, but some of the remaining discrepancies cannot in principle be eliminated within a spherical-ion model. In particular, the effect of spherical breathing on the optical vibrational frequencies is not dramatic and further improvement (e.g., reduction of LO-TO splitting) will require the inclusion of nonspherical charge relaxation (polarizability).

I. INTRODUCTION

Theoretical and experimental investigations into the properties of oxide, fluoride, and sulfide materials have intensified considerably during the last ten years. This is at least partly due to the fact that these materials exhibit a remarkable range of electronic and structural behavior ranging from superconductivity to ferroelectricity and ionic conduction. One step toward unlocking the vast technological potential of such compounds is the development of a thorough understanding of the microscopic mechanisms responsible for the properties of interest. In spite of the many significant advances in the theoretical treatment of condensed-matter systems, oxide materials continue to provide a special challenge. Oxygen anions are typically characterized by rather diffuse electronic charge distributions and, therefore, large polarizabilities, which make quantitative modeling difficult.

In this connection there appears to be an increasingly conspicuous tendency to apply very sophisticated *ab initio* electronic structure computation schemes to the description of oxide materials. This leaves one with the impression that simpler and more approximate methods are totally unreliable or inappropriate. Here we are thinking of, e.g., ionic models, bond-charge models, and so on, as opposed to methods based on a full electronic band structure determination. While there is no doubt that modern quantum molecular-dynamics simulations can provide quite a good accounting of most of the observed properties, they are also known to be extremely time consuming and inefficient, especially for complex structures.

In this work we present a reasonably accurate but very efficient scheme to compute the structural, lattice dynamical, and thermoelastic properties of arbitrarily complex insulating compounds over a range of pressures and temperatures. Our method is derived from an existing class

of approximate *ab initio* schemes developed during the last 20 years[1] which were devised specifically to treat insulating compounds.

Our method exploits the fact that ionic and molecular solids can be modeled, to a first order of approximation, as an assembly of closed-shell units with electronic charge clouds that are more or less localized about their respective nuclei. Approximate density-functional methods can then be used to accurately determine the interaction between the closed-shell atoms or ions. Specifically, the electronic structure of the closed-shell constituents is determined by carrying out a Kohn-Sham[2] density-functional theory (DFT) or a Hartree-Fock calculation. These accurate densities are then used to construct an approximate crystal-charge density, which is in turn used to obtain an estimate of the interaction, or binding energy, using the Gordon-Kim ansatz.[3] Although the latter method is based on simple uniform electron-gas functionals, it is remarkably successful at predicting the short-ranged interaction between closed-shell systems.[4]

The accuracy of methods based on the preceding notions was demonstrated several decades ago by Kim and Gordon[5] who calculated some equilibrium properties of alkali halide crystals. Using free-ion charge densities, they obtained lattice constants and bulk moduli within 8% and 30% of the experimental values, respectively. The same model, in its original rigid-ion formulation, was applied to many alkali halides, alkaline earth halides,[6,7] and fluoride perovskites.[8,9]

An obvious limitation of these original schemes is that they could not be applied to oxide crystals since multiply-charged anions such as O^{2-} are not stable as free ions. This difficulty was ultimately resolved by introducing stabilizing charged spheres around the anions, as originally suggested by Watson in 1958.[10] The "Watson sphere" is intended to simulate the stabilizing field provided by the crystal environment, but the shell radius and charge remain to be determined. The shell radius and charge are often referred to as breathing parameters, although the shell charge is usually fixed (arbitrarily) to neutralize the charge on the anion.

In a model originally introduced by Mulhausen and Gordon[11] and later refined by Hemley and Gordon[12] and Mehl, Hemley, and Boyer,[13] the breathing parameters are subject to plausible but arbitrary (and, strictly speaking, unphysical constraint equations), which couple them to the respective Coulomb-site potentials. In particular, the Watson-sphere radius is adjusted so that the Coulomb potential inside the sphere matches the site potential. This technique, commonly referred to as "potential-induced breathing" (PIB), leads to equations of state that are markedly improved over the rigid-ion results. The method has been applied with varying degrees of success to simple oxides[14] and oxide perovskites.[15,16]

Mulhausen and Gordon[11] were also the first to suggest an alternate scheme based on a variational treatment. In this approach the crystal energy is minimized with respect to the shell radius, which in turn determines the anion-site densities. Unfortunately, the shell radii could not be reliably determined because the crystal energy is extremely flat in the vicinity of the minimum.

Wolf and Bukowinski[17] subsequently showed that a very careful optimization of the Hartree-Fock ionic wave functions must be carried out in order to determine accurate densities and self-energies for each shell radius. They were the first workers to successfully implement variational ionic breathing. In this way many-body effects due to charge-density overlap are approximately included. Their model gave better overall agreement with experimental data for the static and elastic properties of MgO and CaO than any previous electron-gas model.

In a very recent study, Zhang and Bukowinski[18] (ZB) calculated the equations of state and static properties of a number of alkaline earth cubic oxides using a "self-consistent" crystal potential scheme. Their breathing potential is also that due to a Watson sphere, but with the inner potential replaced by the spherical average of the crystal potential [local-density approximation (LDA) exchange correlation + Coulomb] obtained from ionic charge densities and the Watson-sphere parameters obtained from a self-consistent scheme. Using this modified PIB (MPIB) method, ZB were able to very accurately reproduce the observed equations of state and phase stability of a number of alkali halides and cubic oxides. While their method retains a certain degree of simplicity through the use of the Gordon-Kim ansatz with Watson-spherelike stabilizing potentials, its self-consistent character vitiates a simple description for the formulation of lattice dynamics within this model, as discussed below.

It is straightforward to set up and solve the general lattice dynamics equations for the simple rigid-ion electron-gas models. With these models it is typically found that the "averaged" vibrational properties of an ionic crystal are adequately represented. In detail, however, all of the expected deficiencies of rigid-ion dynamics are manifest. These include a predicted observance of the Cauchy relations for the elastic constants (i.e., $C_{12}=C_{44}$ for cubic crystals), in contradiction with experiment, and a substantial overestimate of the splitting between longitudinal optic (LO) and transverse optic (TO) mode frequencies.

Semiempirical lattice dynamic models have demonstrated that the reduction of LO-TO splitting in real materials (relative to the rigid-ion value) can be related to an induced dipolar polarization of the ions, whereas the observed deviations from the Cauchy relations is at least partly due to nondipolar deformations. Both problems have been treated separately. Dipolar deformations were introduced by Basu and Sengupta,[19] who used perturbative estimates for the ionic wave functions and electron-gas potentials to determine the parameters for a simple shell model. Although their model is based on simplifying assumptions such as the point-dipole approximation, it yields dispersion relations for alkali halides that are in very good agreement with experiment. A shell-model approach was also introduced by Jackson and Gordon[20] to simulate the static structural properties of SiO_2 quartz. In their method, split shells on the oxygen ions were used, thus allowing both dipolar and quadrupolar deformations. More recently, Lacks and Gordon[21,22] have performed calculations using the so-called polarization-

included breathing electron-gas (PEG) model. The prescription is similar in spirit to the variationally-induced breathing (VIB) approach, but is based on Hartree-Fock densities in the Gordon-Kim ansatz. To simulate the nonspherical environment around anions, these authors introduce point charges in place of the Watson sphere. Charge relaxation is achieved by supplementing the Hartree-Fock basis sets with floating tetrahedral lobe functions localized along bond directions. The point-charge positions and the exponents and locations of the Gaussian functions are then varied for each structural configuration, until a minimum in the total static crystal energy is obtained. The crystal property predictions obtained using this latter approach are very encouraging and typically (but not exclusively[21]) surpass their MEG counterparts in terms of accuracy. Unfortunately, neither of the methodologies discussed above have yet been applied to the calculation vibrational modes or elastic constants.

Apart from the perturbative dipolar deformation explored by Basu and Sengupta,[19] the only other charge-density deformation that has been included in electron-gas lattice dynamical modeling of crystals has been spherical-ion breathing. Spherical deformation of the anion-charge densities in electron-gas models has been found to be an important many-body effect in oxides. The inclusion of spherical breathing is crucial to obtain a realistic description of the structural response of oxides to applied pressure. Both the PIB and Wolf-Bukowinski (WB) variational models reasonably reproduce the observed violations of the Cauchy relations for cubic alkaline earth oxides. The lattice dynamics of the PIB model was presented[23] by Cohen, Boyer, and Mehl and applied to a number of oxide materials. However, the significant reduction in the LO-TO splitting calculated using the PIB model for the alkaline earth oxides underscores the unphysical basis of this model. In the long-wavelength limit, the additional restoring force acting on the ions in the LO mode is due to the presence of a linear macroscopic electric field. Physically, this linear field cannot couple to spherical breathing modes. Hence spherical breathing in an ionic model should give the same degree of LO-TO splitting as any rigid-ion model. The reduction in LO-TO splitting which arises in PIB results from the unphysical constraint equations imposed by the PIB ansatz; i.e., the Watson-sphere parameters are determined by the Coulomb-site potential (we will address this point in more detail in Sec. IV B).

In this paper we more fully develop the work of Wolf and Bukowinski[17] by deriving the dynamical matrix for the variational electron-gas model within the spherical-ion approximation. In this variationally-induced breathing (VIB) model, the electronic variational parameters are treated as dynamical variables within the adiabatic approximation. Similar to PIB, the ionic charge densities spherically deform under lattice vibrations, but in contrast to PIB the electronic breathing parameters minimize the total energy.

With the computed phonon density of states, the structural parameters of a crystal can then be determined at any temperature and pressure (or stress condition) by minimizing the quasiharmonic Gibbs free energy with respect to the structural parameters along the electronic adiabatic surface. The complete pressure- and temperature-dependent thermoelastic properties of a crystal an also be determined. We have applied the VIB procedure to calculate the equations of state, elastic properties, phonon dispersion relations, and phase stability of several alkaline earth oxides (MgO, CaO, and SrO). The calculated properties are generally in quite good agreement with experiment.

Spherical charge deformation within the VIB ionic description is responsible for a substantial improvement over rigid-ion elastic constants and bulk moduli. However, some of the remaining discrepancies cannot in principle be eliminated within a spherical-ion model. In particular, the effect of spherical breathing on the optical vibrational frequencies is not dramatic and further improvement (e.g., reduction of LO-TO splitting) will require the inclusion of nonspherical charge relaxation (polarizability).

We have also explored several ways of optimizing the effectiveness of spherical breathing in the VIB procedure. In particular, we have evaluated the effect of using different analytical forms for the potential used to stabilize the oxygen-charge density. In addition, we have also investigated the importance of anion-cation charge transfer within the variational scheme. An important technical difference between the original WB variational model and the VIB model presented here is that the ionic charge densities are computed using a numerical Kohn-Sham procedure rather than using a Hartree-Fock orbital prescription. This modification increases the speed of the calculation enormously without the added complications of basis set dependences.

II. GENERAL THEORY

In this section we outline the philosophy and formalism of the VIB approach to crystal statics and dynamics. The organization is as follows: We being by describing in broad terms the fundamental underlying physical concepts of the theory, emphasizing its application to ionic crystals. We then briefly review the Gordon-Kim approximation for calculating interactions. Finally, we provide a detailed theoretical description of VIB statics and dynamics.

A. Philosophy of the VIB model

When ions (or atoms) are assembled into a crystal, a certain degree of charge rearrangement takes place. This is most evident in metals and almost negligible in the case of many ionic compounds (for example, the alkali halides). In the latter case it is well known that the crystal density is very well represented by the sum of its constituent ion's closed-shell densities. Within the class of ionic solids, the most striking charge rearrangement occurs in oxides since O^{2-} is not stable as a free ion. In this case the crystal potential including overlap interactions must be simulated in the atomic calculation. This is customarily done by adding to the nuclear potential that of a charged sphere with radius R_w and charge Q_w on its

surface and then solving the atomic Kohn-Sham problem in the resulting potential. As pointed out in the Introduction, this technique, which was introduced by Watson[10] for the treatment of Hartree-Fock ions, also provides a convenient mechanism for spherical breathing. Such a Watson sphere is simply introduced around every ion that is allowed to deform (not limited to oxygen), and both the radius and charge of the sphere can then be taken as variational parameters that determine the size of the ion. In fact, any parameters that define the electronic charge density of the ions can be used as variational parameters. We will denote the general set of such electronic variational parameters by ζ.

By representing the total crystal density as a superposition of such variational site ionic densities, the total interaction energy takes the form

$$\Phi_{\text{total}}=E\left[\sum_i n_i^{\zeta}\right]-\sum_i E[n_i^0]\ , \tag{1}$$

where n_i^{ζ} and n_i^0 are, respectively, the fragment charge densities in their crystal and free states. According to density-functional theory the ground-state energy, as well as the corresponding ground-state density, can be obtained by minimizing the energy expressions with respect to the charge density. The VIB procedure exploits this principle, but provides an estimate of the ground-state energy given a variational ansatz for the total crystal density.

There are two distinct aspects to the implementation of VIB: the mechanism responsible for the electronic site charge deformations and the accounting of the concomitant energy costs. The latter can be broken down into overlap and self-energy effects. In particular, as the charge densities on neighboring sites deform (given a fixed internuclear separation), the short-ranged overlap interactions are modified. An additional energy contribution comes from the change in the electronic self-energy of the distorted ion relative to the free-ion state. This notion can be formalized by recasting (1) into the form

$$\Phi_{\text{total}}=\left\{E\left[\sum_i n_i^{\zeta}\right]-\sum_i E[n_i^{\zeta}]\right\}+\left\{\sum_i (E[n_i^{\zeta}]-E[n_i^0])\right\}\ . \tag{2}$$

This expression can be further simplified when the electronic charge densities of the fragments do not overlap strongly. In this case the first term can be replaced by a pairwise summation. In practice, this approximation is quite good even in the case of the oxide crystals considered since it leads to a change in the zero-pressure volume of less than a few percent.[11] The simplified expression takes the form

$$\Phi_{\text{total}}\simeq\sum_{i>j}\left[E[n_i^{\zeta}+n_j^{\zeta}]-E[n_i^{\zeta}]-E[n_j^{\zeta}]\right]+\left\{\sum_i (E[n_i^{\zeta}]-E[n_i^0])\right\}\ . \tag{3}$$

In this formula the first term represents *all* the crystal interactions between the deformed fragments including point-ionic Coulomb interactions. The second term accounts for the energy cost associated with the distortion of the fragments relative to their dissociated reference state.

While the preceding formula implies that the same energy functional is used to evaluate all the energy contributions, yet another approximation is made in practice. In particular, the short-ranged interactions contained in the first term on the right-hand side are evaluated using the Thomas-Fermi-like Gordon-Kim (GK) approximation (discussed below). However, functionals of this kind do not represent the electronic kinetic-energy contributions to the total energies of the individual ions very accurately. This is at least partly due to the fact that the charge density varies more rapidly in the core regions of atoms (which harbor most of the self-energy), but is much more homogeneous in the outer regions which mediate the overlap interaction. For this reason fully self-consistent Kohn-Sham calculations are performed in order to generate reliable self-energies. As a by-product, realistic ionic charge densities are also obtained for input into the Gordon-Kim interaction formula.

The essence of the VIB approach is to minimize the total crystal energy with respect to both the distortion parameters ζ and the lattice structural parameters **R**. For computational simplicity we restrict ourselves here to variational parameters that deform the ions spherically. The main purpose is to show how important it is to include variational parameters in electron-gas models by demonstrating the effect of spherical breathing on the model's predictions for those crystal properties that couple to the breathing degrees of freedom. It will be pointed out throughout the paper wherever this restriction to spherically symmetric ions seems to be inadequate and additional variational parameters that allow for nonspherical deformations of the ions need to be included.

Figure 1 illustrates the effect of spherical breathing on the Kohn-Sham $O^{2-1}(^1S;\zeta)$ charge density. As can be seen from the plot, the ionic core is practically unperturbed; only the tail of the charge distribution is expanded or contracted in accord with the breathing parameters. The range of variability shown is typical for the range of temperatures and pressures simulated in our calculations of oxide material properties. The formal and computational details of the breathing mechanism will be discussed in detail below.

B. DFT approach to energetics

One of the obvious advantages of the GK approach is that it is extremely efficient computationally. To exploit this scheme, however, an input density ansatz is required. In the original formulation of Gordon and Kim, the component charge fragments were rigid ions with radially symmetric charge distributions derived from Hartree-Fock wave functions for isolated closed-shell ions. A superposition of such spherical densities was used as an approximation to the actual interacting density. In the present work we use a variant of the original GK scheme in which the input densities are obtained from a superpo-

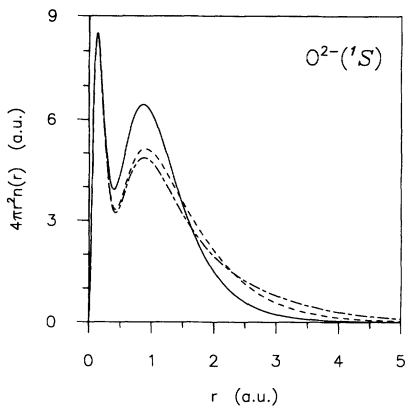

FIG. 1. Example of spherical breathing on the oxygen charge density. Kohn-Sham calculations were performed for a Watson-sphere-stabilized ion with a Watson charge of $Q_w = +2.0e$ and variable Watson radius R_w. Solid line, $R_w = 1$ a.u.; dashed line, $R_w = 2$ a.u.; dot-dashed line, $R_w = 3$ a.u.

sition of Kohn-Sham densities. For completeness and to establish our notation, we therefore first provide a brief review of DFT followed by a discussion of the GK scheme.

The density-functional formalism is based on a theorem due to Hohenberg and Kohn[24] (HK), which states that the ground-state energy of an electronic system is expressible as a functional of the electron density, namely,

$$E[n]=T[n]+\frac{1}{2}\int d\mathbf{r}\, n(\mathbf{r})\phi(\mathbf{r})+E^{\mathrm{xc}}[n] + \int d\mathbf{r}\, n(\mathbf{r})v_{\mathrm{ext}}(\mathbf{r}) , \tag{4}$$

where $\phi(\mathbf{r})$ is the electrostatic potential associated with the density $n(\mathbf{r})$. The first three terms represent, respectively, the kinetic energy of the noninteracting system, the classical electron-electron repulsion, and the exchange-correlation energy. Together they form a universal functional which defines *all* the electronic interactions within the system. The fourth term represents the interaction of the electrons with their external environment (i.e., nuclei) and changes from one electronic structure problem to the next.

Unfortunately, the functionals above are only explicitly known in certain limiting cases. The kinetic-energy functional $T[n]$, for instance, is only exactly known for a uniform electron-density distribution and for a relatively small number of sufficiently simple model systems. The same is true for the exchange and correlation energy functional. Thomas-Fermi-like theories are based on the use of the uniform electron-gas functionals for both the kinetic and exchange functionals. The kinetic and exchange energies per unit volume in a uniform system are constants characterized by the value of the density or, equivalently, the r_s value defined by $n=1/(\frac{4}{3}\pi r_s^3)$. The corresponding density functionals are obtained by applying the local-density approximation (LDA), which amounts to ascribing a coordinate dependence to the density parameter n. For the kinetic and exchange energies, the results take the form

$$T_0[n]=\tfrac{3}{10}(3\pi^2)^{2/3}\int d\mathbf{r}\, n(\mathbf{r})^{5/3} \tag{5}$$

and

$$E_0^X[n]=-\frac{3}{4}\left[\frac{3}{\pi}\right]^{1/3}\int d\mathbf{r}\, n(\mathbf{r})^{4/3} . \tag{6}$$

Correlation energy functionals for a uniform electron gas have also been put forward by a number of workers. However, our aim here is not to review the advances in DFT and the treatment of correlation energy, but to provide a measure of reference for subsequent discussion. A frequently employed approximation, and one we shall use in the calculations to be presented, is that of Gunnarsson and Lundqvist.[25] Other functionals for the correlation energy can also be used, but do not materially alter any of our results. We shall briefly discuss the importance of intrasystem and intersystem correlation effects in Sec. IV.

Let us now consider the interaction between a single pair of quantum-mechanical fragments. In the present work we shall be concerned exclusively with estimating the crystal interactions via such pair interactions. Within the DFT framework the interaction energy is formally given by

$$\Delta E_{12}=E[n]-E[n_1]-E[n_2] , \tag{7}$$

where n denotes the ground-state density of the combined interacting system and n_1 and n_2 represent the ground-state densities of the isolated fragments. Within the Gordon-Kim prescription[3,5] the generalized Thomas-Fermi (GTF) functional

$$E^{\mathrm{GTF}}[n]=T_0[n]+\frac{1}{2}\int d\mathbf{r}\int d\mathbf{r}'\frac{n(\mathbf{r})n(\mathbf{r}')}{|\mathbf{r}-\mathbf{r}'|} + E_0^X[n]+E^C[n] \tag{8}$$

is used to estimate the pair interactions. The GK formula is obtained by invoking the additivity assumption and using, in place of the GTF densities appropriate to E^{GTF}, those obtained from a Kohn-Sham[2] or Hartree-Fock atomic calculation. The expression for the approximate interaction then takes the form

$$\Delta E_{12}^{\mathrm{GK}}=\Delta T_0+\int d\mathbf{r}\,\phi_1(\mathbf{r})n_2(\mathbf{r})+\Delta E_0^X + \Delta E_0^C+\Delta E^{\mathrm{nuc}} , \tag{9}$$

where ϕ_1 is the electrostatic potential due to the electronic charge n_1, ΔE^{nuc} represents nuclear repulsion, and, for example, $\Delta T_0=T_0[n_1+n_2]-T_0[n_1]-T_0[n_2]$. Similar expressions hold for ΔE_0^X and ΔE_0^C. It should be pointed out that the formal error in this interaction energy estimate is of order δn, the deviation of the input density away from the true GTF ground-state density n^{GTF}. Thus, in the case of neutral atoms, $E^{\mathrm{GTF}}[n^{\mathrm{KS}}]$ actually provides an inferior estimate of the ground-state energy compared to $E^{\mathrm{GTF}}[n^{\mathrm{GTF}}]$, although the input density is presumably more realistic. Nevertheless, the original work[3,5] of GK shows that Eq. (9), when applied to closed-shell interactions, yields surprisingly accurate estimates. Ultimately, this suggests that the errors arising

from the various approximations cancel in some nontrivial way.[26]

Shortly after its appearance in the literature, a number of attempts were made to improve the GK scheme by extending the basic GTF functional to include gradient corrections to the kinetic and exchange energies. One of the first attempts at such an extension is due to Shih[27] who incorporated the von Weiszacker correction in the GK prescription. Although the corrected functional leads to substantially improved estimates for individual atoms and ions[28–30] Shih finds the von Weiszacker contribution to the *interaction* to be dominant at long range and *negative* compared to the uniform electron-gas term. Shih speculates that the poor results obtained from this procedure are due to a failure of the additivity assumption used to construct the input densities for the gradient-corrected functionals. Subsequently, Pearson and Gordon[31] (PG) reconsidered the inclusion of gradient corrections by applying a local truncation to the kinetic-energy volume density, rather than the actual kinetic-energy functional. Using a somewhat *ad hoc* truncation prescription, they find only marginal improvements in the interaction estimates.

Using the VIB procedure, we have also applied both the gradient expansions as in Shih's work, and the PG truncation procedure to the calculation of our ionic interactions. In both cases we find substantial discrepancies between our calculated equations of state and equilibrium volumes and those obtained by applying the presumably cruder GK prescription. Similar conclusions were obtained by Lacks and Gordon[32] who recently compared the performance of various gradient-corrected kinetic-energy functionals. Although the kinetic-energy estimates for isolated constituents can be somewhat improved by the inclusion of gradient terms, the latter authors also find that the interatomic interactions are worsened. This would seem to imply that the error cancellations inherent in the GK ansatz may indeed be fortuitous. We have chosen to work with a variant of the original Gordon-Kim interaction formula in which the ionic fragment densities are computed using the Kohn-Sham (KS) procedure, including exchange *and* correlation, but in which the interaction (9) is calculated using KS exchange only, in including a correlation contribution. In a subsequent section we shall make contact with a recent study by Illas *et al.*,[33] which provides some justification for this choice. We find that the neglect of correlation energy in the Gordon-Kim treatment of the interaction leads to systematic improvements in the calculated properties of alkaline earth oxides.

C. Lattice statics

In the VIB model the total binding energy of the static crystal, as given in Eq. (3), can be expressed as

$$\Phi=\sum_{i<j}\left[\frac{I_iI_j}{R_{ij}}+\Phi_{ij}(R_{ij},\zeta_i,\zeta_j)\right]+\sum_i\Phi_i^s(\zeta_i)\ . \tag{10}$$

The first term, which contains all the crystal interactions, has now been written as the sum of two terms. The first of these represents the point-ion Madelung energy. Here i and j label the ions of the crystal, R_{ij} is the separation between ions i and j, and the I's stand for the ionic charges. The Madelung energy is obtained by summing up the long-ranged point-ion electrostatic interactions using Ewald's method.[34] The second term in the brackets, Φ_{ij}, is the short-ranged interaction energy. The last term in this definition, Φ_i^s, is the contribution to the binding energy due to the change in the ionic self-energies. We now discuss these latter two contributions in more detail.

The short-ranged overlap interaction can be split into three parts:

$$\Phi_{ij}=\Delta E_{ij}^{\rm SRC}+\Delta T_{ij}+\Delta E_{ij}^{X}\ . \tag{11}$$

$\Delta E_{ij}^{\rm SRC}$ is the short-ranged Coulombic term that is due to overlapping charge densities. It is given by the exact electrostatic interaction between two spatially-extended charge distributions minus the long-ranged point-ion Coulomb energy:

$$\Delta E_{ij}^{\rm SRC}=\frac{Z_iZ_j-I_iI_j}{|\mathbf{R}_i-\mathbf{R}_j|}+\int d\mathbf{r}\int d\mathbf{r}'\frac{n_i^{\zeta}(\mathbf{r})n_j^{\zeta}(\mathbf{r}')}{|\mathbf{r}-\mathbf{r}'|}-Z_i\int d\mathbf{r}\frac{n_j^{\zeta}(\mathbf{r})}{|\mathbf{r}-\mathbf{R}_i|}-Z_j\int d\mathbf{r}\frac{n_i^{\zeta}(\mathbf{r})}{|\mathbf{r}-\mathbf{R}_j|}\ . \tag{12}$$

Here Z is the nuclear charge and I the total charge of the respective ion; $n(\mathbf{r})$ is its electronic charge density, and $\mathbf{R}$ is the position of its nucleus. The remaining kinetic and exchange contributions are calculated using the GK procedure as described previously.

We now discuss the calculation of the distorted charge densities and their corresponding self-energies. Both are obtained simultaneously by solving the Kohn-Sham problem self-consistently at each site in the crystal subject to an effective local many-body potential (ELMBP) $W(\zeta^i;\mathbf{r})$. The ELMBP provides the breathing mechanism and ionic stabilization (if required). Although $W(\zeta^i;\mathbf{r})$ is usually taken to be a Watson sphere with variable radius and charge, more flexible parametrizations can easily be implemented (see Sec. IV). In this case the single-particle Kohn-Sham problem can be written as

$$\{-\tfrac{1}{2}\nabla^2+v_{\rm eff}[n_i^{\zeta}]+W(\mathbf{r};\zeta_i)\}\phi_m^i=\varepsilon_m^i\phi_m^i\ , \tag{13}$$

where m is the state label and the index i labels the site in the crystal. The electronic self-energy associated with the ion at site i is then obtained by subtracting from the Kohn-Sham ground-state energy the interaction of the density with its ELMBP,

$$E_i^s(\zeta_i)=E_{\rm KS}[(n_i^{\zeta})]-\int d\mathbf{r}\,n_i^{\zeta}(\mathbf{r})W(\mathbf{r};\zeta_i)\ . \tag{14}$$

This crucial step is required in order to avoid double counting the ions' interaction with its local electronic environment. With this definition *all* the crystal interactions are contained in the first term on the right-hand side of Eq. (10), while the second term measures the cost in electronic self-energy due to charge relaxation. The change in the self-energy is therefore defined by

$$\Phi_i^s(\zeta_i)=E_i^s(\zeta_i)-E_i^s(\zeta_i^0)\ . \tag{15}$$

The particular choice of reference state ζ_i^0 used to

define the self-energy is immaterial. In our calculations the reference state is a Watson-sphere-stabilized O^{2-} ion with $R_w = 2.15$ a.u. and $Q_w = +2.0e$. The corresponding self-energy of $O^{2-}(^1S;\zeta_i^0) = -74.373\,453$ a.u. Since O^{2-} is not stable as a free ion, to obtain the binding energies of the crystal, the Kohn-Sham energy associated with the reaction

$$O^{2-}(^1S;\zeta_i^0) \rightarrow O^-(^2P) + e^- \tag{16}$$

was calculated. For the reference state $\zeta_i^0 = (R_w = 2.15, Q_w = 2.0)$, the energy of this reaction was determined to be $-0.369\,26$ a.u. This value is then *subtracted* from the binding energy obtained from a VIB calculation to yield the dissociation energy of the crystal.

The equation of state and certain equilibrium properties of the static lattice can be obtained as a function of pressure (or any general strain tensor) by minimizing the Gibbs free energy of the static crystal, $G_{\text{static}} = \Phi + pV$, with respect to the lattice structural parameters $\mathbf{R}$. The free-energy minimization is performed along an adiabatic energy surface where the total electronic energy is at a minimum with respect to the variational parameters, i.e.,

$$G_{\text{static}}(p) = \min_{\mathbf{R}} \{ \min_{\zeta} [\Phi(\mathbf{R};\zeta)] + pV(\mathbf{R}) \} . \tag{17}$$

The short-ranged contribution to Φ was obtained by direct lattice sums over the first three coordination shells of each ion.

D. Lattice dynamics

The dynamical matrix in the VIB model is derived by treating the electronic variational parameters as dynamical variables subject to the adiabatic condition. As in empirical shell models,[35,36] the equations of motion in the quasiharmonic approximation are obtained by expanding the static lattice energy Φ of Eq. (10) up to second order in the nuclear displacements $\mathbf{u}$ and variations $\mathbf{v}$ of the breathing parameters of all the ions (in matrix notation):

$$\Phi = \Phi_0 + \Phi^R \mathbf{u} + \Phi^\zeta \mathbf{v} + \tfrac{1}{2}\mathbf{u}\Phi^{RR}\mathbf{u} + \tfrac{1}{2}\mathbf{u}\Phi^{R\zeta}\mathbf{v} + \tfrac{1}{2}\mathbf{v}\Phi^{\zeta R}\mathbf{u} + \tfrac{1}{2}\mathbf{v}\Phi^{\zeta\zeta}\mathbf{v} . \tag{18}$$

Here Φ_0 represents the potential energy of the equilibrium static lattice. Φ^R and Φ^ζ are the multidimensional gradients of Φ with respect to all the nuclear coordinates $\mathbf{R}$ and all the breathing parameters ζ, respectively, and Φ^{RR}, $\Phi^{R\zeta}$, $\Phi^{\zeta R}$, and $\Phi^{\zeta\zeta}$ are the respective (second derivative) force-constant matrices. If the expansion is made at the equilibrium configuration, the linear terms vanish and the equations of motion can be written as the following set of coupled equations involving the nuclear and electronic coordinates:

$$-\mathbf{M}\ddot{\mathbf{u}} = \Phi^{RR}\mathbf{u} + \Phi^{R\zeta}\mathbf{v} , \tag{19}$$

$$0 = \Phi^{\zeta R}\mathbf{u} + \Phi^{\zeta\zeta}\mathbf{v} . \tag{20}$$

$\mathbf{M}$ is a diagonal $(3Nn \times 3Nn)$ matrix (N = total number of primitive cells and n = number of ions in the primitive cell) containing the ionic masses as elements. In Eq. (20) we have made the adiabatic approximation by setting the masses associated with the breathing variables, which represent electronic degrees of freedom, to zero. With these coupled equations given, the equations of motion for the Fourier-transformed variables $\mathbf{u}(\mathbf{q})$ and $\mathbf{v}(\mathbf{q})$ decouple into N independent sets of equations, one (coupled) set for every wave vector $\mathbf{q}$:

$$-\mathbf{M}\ddot{\mathbf{u}}(\mathbf{q}) = \mathcal{D}^{RR}(\mathbf{q})\mathbf{u}(\mathbf{q}) + \mathcal{D}^{R\zeta}(\mathbf{q})\mathbf{v}(\mathbf{q}) , \tag{21}$$

$$0 = \mathcal{D}^{\zeta R}(\mathbf{q})\mathbf{u}(\mathbf{q}) + \mathcal{D}^{\zeta\zeta}(\mathbf{q})\mathbf{v}(\mathbf{q}) . \tag{22}$$

Here M is a diagonal $(3n \times 3n)$ matrix containing the ionic masses, and the $\mathcal{D}$ matrices are the $\mathbf{q}$ components of the Fourier transforms of the respective force-constant matrices. To derive Eqs. (21) and (22), we have assumed periodic boundary conditions and have made use of the translational symmetry of the force constants. Equation (22) is solved for $\mathbf{v}(\mathbf{q})$, which is then inserted into Eq. (21) to obtain the general equation of motion for the nuclear coordinates,

$$-\ddot{\mathbf{u}}(\mathbf{q}) = \mathbf{M}^{-1}\{\mathcal{D}^{RR}(\mathbf{q}) - \mathcal{D}^{R\zeta}(\mathbf{q})[\mathcal{D}^{\zeta\zeta}(\mathbf{q})]^{-1}\mathcal{D}^{\zeta R}(\mathbf{q})\}\mathbf{u}(\mathbf{q}) . \tag{23}$$

$\mathcal{D}^{\zeta\zeta}(\mathbf{q})$ is a Hermitian $(m \times m)$ matrix (m = number of breathing parameters per unit cell) and is easily inverted numerically. The $\mathcal{D}^{RR}$ part of the dynamical matrix is the rigid-ion contribution and consists of the short-ranged rigid-ion overlap part and the long-ranged Coulomb (or Kellermann) matrix, which is calculated using Ewald's method.[34,37] The other contributions $\mathcal{D}^{R\zeta}$ and $\mathcal{D}^{\zeta R}$ are the direct coupling terms between the electronic and nuclear coordinates. The latter contributions are of a short-ranged nature and can be calculated by direct lattice summation. Explicit expressions for the short-ranged potential contributions to the various dynamical matrix elements are provided in the Appendix.

To obtain the equations of state at finite temperatures, we invoke the quasiharmonic approximation;[38] i.e., at temperature T the thermal contribution to the energy for a given structural configuration is that given by the corresponding harmonic system. In the quasiharmonic approximation the formulas for the vibrational energy E_{th} and free energy G_{th} are given, respectively, by

$$G_{\text{th}}(\mathbf{R},t;\zeta_{ad}) = \sum_i [\tfrac{1}{2}\hbar\omega_i + k_B T \ln(1 - e^{-\hbar\omega_i/k_B T})] \tag{24}$$

and

$$E_{\text{th}}(\mathbf{R},T;\zeta_{ad}) = \Phi_0(\mathbf{R}) + \sum_i \left[\frac{1}{2}\hbar\omega_i + \frac{\hbar\omega_i e^{-\hbar\omega_i/k_B T}}{1 - e^{-\hbar\omega_i/k_B T}} \right] . \tag{25}$$

Here the ω_i are the quasiharmonic normal-mode frequencies associated with the structural configuration, k_B is Boltzmann's constant, and the sums are formally over all the normal modes of the lattice. The mode frequencies implicitly depend on ζ_{ad}, the values of the electronic variational parameters that minimize Φ_0. Given a pressure p and a temperature T, the equilibrium structural

parameters **R** are those that minimize the total quasiharmonic Gibbs free energy along the adiabatic electronic surface:

$$G(T,p)=\min_{\mathbf{R}}\{\min_{\zeta}[\Phi(\mathbf{r};\zeta)]+G_{\rm th}(\mathbf{R},T;\zeta_{ad})+pV(\mathbf{R})\}\ . \tag{26}$$

III. COMPUTATIONAL DETAILS

In this section we describe some of the computational procedures followed for the calculations outlined in the previous section.

As pointed out earlier in the text, we employ the Kohn-Sham procedure to obtain the ionic charge densities. To implement VIB our basic Kohn-Sham code was modified to include, in addition to the usual nuclear external potential, the ELMBP $W(\mathbf{r};\zeta_i)$. When this potential is chosen to be a Watson sphere, the integration mesh must be scaled in such a way that the discontinuity in the potential at $r=R_w$ matches a mesh point. In practice, we have found that the small differences in the self-energy resulting from the neglect of this matching procedure can adversely affect the convergence of the crystal energy minimization. We typically employ a Herman-Skillman mesh with 10 blocks, 48 points per block, and a typical initial step size of 0.001 atomic units. For the exchange-correlation functional we use the form proposed by Gunnarsson and Lundqvist.[25] From the resulting ionic charge densities, the short-ranged overlap pair-interaction potentials (in the following just "pair potentials") were calculated according to Eq. (11) by numerical integration. The contributions to Φ_{ij} were combined in a single integrand, and a (24×32)-point Gauss-Legendre integration in spheroidal coordinates yielded results for the pair potentials that were fully converged.

The calculation of the dynamical matrices in Eq. (23) involves various derivatives of the total energy Eq. (10) with respect to the nuclear coordinates and the variational parameters, which makes it necessary to differentiate the pair potentials Φ_{ij} and the self-energy Φ^s. As an example, consider the case of two interacting ions both with Watson spheres. In general, the pair potentials are functions of five variables: the separation r of the ions and two breathing parameters (R_w and Q_w) for each of the ions. We considered two practical schemes for extracting the mixed partial derivative information from this type of multidimensional potential-energy surface (PES). In the first, we fitted the various potentials to an analytic form that could be explicitly differentiated. However, optimizing the various coefficients and exponents of the analytic equations turned out to be a formidable task for such a complicated multiparameter function. For this reason, and because the fitting procedure would have to be repeated for each new system, we abandoned this approach. We decided, instead, to construct multidimensional splines for the PES. Splines not only provide smooth derivative information, but have the advantage that they are relatively robust, so that the procedure of generating derivatives for an arbitrary system's PES can be automated.

Ultimately, however, the complexity involved in using multidimensional splines can also be avoided. As we shall show in Sec. IV C below, a Watson-sphere potential with variable R_w and a frozen but judiciously chosen Q_w yield essentially the same results as obtained from more elaborate variational forms. In additional, the cation-cation and anion-cation pair PES's can be further simplified since we find that the deformation of the cation-charge densities in their crystal environment is insignificant. With this assumption the anion-cation pair interactions depend on only two parameters, r and a single R_w on the anion, while the cation-cation potentials depend only on r. These simplifications of the parametric dependence permits the implementation of standard bicubic spline interpolation, which is sufficiently efficient and accurate to be used in our application.

An additional complication arises in connection with the anion-anion pair potentials $\phi(r,\zeta_1,\zeta_2)$ which are, in general, functions of *two* independent breathing variables. This difficulty can be resolved by introducing the new parameters $\varepsilon=\frac{1}{2}(\zeta_1-\zeta_2)$ and $\zeta=\frac{1}{2}(\zeta_1+\zeta_2)$ and expanding the anion-anion potentials as follows:

$$\begin{aligned}\phi(r,\zeta-\varepsilon,\zeta+\varepsilon)&=\phi(r,\zeta,\zeta)+\left.\frac{d\phi(r,\zeta-\varepsilon,\zeta+\varepsilon)}{d\varepsilon}\right|_{\varepsilon=0}\varepsilon\\&\quad+\frac{1}{2}\left.\frac{d^2\phi(r,\zeta-\varepsilon,\zeta+\varepsilon)}{d\varepsilon^2}\right|_{\varepsilon=0}\varepsilon^2+\cdots\\&=f(r,\zeta)+\tfrac{1}{2}g(r,\zeta)\varepsilon^2\ ,\end{aligned} \tag{27}$$

where

$$\begin{aligned}f(r,\zeta)&\equiv\phi(r,\zeta,\zeta)\ ,\\ g(r,\zeta)&\equiv\frac{d^2}{d\varepsilon^2}\phi(r,\zeta+\varepsilon,\zeta-\varepsilon)|_{\varepsilon=0}\ .\end{aligned} \tag{28}$$

The first derivative term in Eq. (27) vanishes from symmetry considerations the calculation of the function $g(r,\zeta)$ involves, taking finite-difference second derivatives with a small value of $\varepsilon\simeq0.01$. This function represents the contribution to the anion-anion interaction for slightly inequivalent ELMBP's. The second derivatives of the anion-anion pair potentials needed for the dynamical matrix calculation were then determined from these functions according to the formulas

$$\begin{aligned}\frac{\partial^2\phi}{\partial r\,\partial\zeta_i}&=\frac{1}{2}\frac{\partial^2 f}{\partial r\,\partial\zeta}\ ,\\ \frac{\partial^2\phi}{\partial\zeta_i^2}&=\frac{1}{4}\left[\frac{\partial^2 f}{\partial\zeta^2}+g\right]\ ,\\ \frac{\partial^2\phi}{\partial\zeta_i\zeta_j}&=\frac{1}{4}\left[\frac{\partial^2 f}{\partial\zeta^2}-g\right]\ .\end{aligned} \tag{29}$$

For the systems considered here, the PES was computed over the range 1.0–13.0 a.u. for r and 1.0–3.0 a.u. for ζ. The crystal energy minimizations were carried out using a Simplex procedure[39] with an energy tolerence of 10^{-8} a.u.

IV. RESULTS AND DISCUSSION

A. Static and elastic properties

The VIB predictions for the binding energies, lattice constants, and elastic properties of MgO, CaO, and SrO at 300 K and zero pressure are summarized in Table I where they are compared to experimental values. All calculations were performed using a Watson sphere on the oxygen ions with R_w as the only variational parameter and a frozen value of $Q_w = +2.0e$. For all three materials, the $B1$ (sodium chloride) structure is correctly predicted to be dynamically stable and lower in energy than the $B2$ (cesium chloride) structure at zero pressure. The calculated dissociation energies of the $B1$ structure are all within 5% of the experimental values. For the $B1$ structure the calculated lattice constants (at ambient pressure) are all within 2% of experimental values. The calculated (isothermal) bulk moduli and their pressure derivatives are of comparable accuracy and differ from the experimental values by less than 2%. The accuracy of these results is remarkable in view of the fact that neither nonspherical charge relaxation nor charge transfer were included in these calculations. In contrast, the bulk moduli calculated using the rigid-ion model (obtained by freezing the breathing parameter R_w at its VIB equilibrium value) are overestimated by 58% for MgO, 34% for CaO, and 36% for SrO. The magnitude of this softening effect of variational ionic breathing demonstrates the importance of including spherical charge relaxation in electron-gas models.

The calculated equations of state of the $B1$ and $B2$ structures at 300 K are compared with the available experimental data for MgO, CaO, and SrO in Figs. 2, 3, and 4. The equation of state for MgO matches the data very well. For CaO and SrO the calculated volumes for the $B1$ structure are below experimental values by about 6% over the entire pressure range. For the $B2$ structure, however, the calculated values are in much better agreement with the data. These results imply that the highly accurate VIB predictions for the MgO $B1$ equation of state may not reflect the overall accuracy of the model and that volume errors on the order of 6% may be more representative.

The phase-transition pressures for the $B1$-$B2$ structures were also calculated. For MgO, VIB predicts a $B1$-$B2$ transition at 420 GPa, which is consistent with the available data that show the $B1$ phase to be stable up to at least 200 GPa.[40] The calculated transition pressure for CaO is 139 GPa, considerably higher than the experimental value of 63 GPa.[41] For SrO the predicted $B1$-$B2$ transition is at 100 GPa, again much higher than the experimental value of 36 GPa.[42,43]

The overestimate in the $B1$-$B2$ transition pressures for CaO and SrO arises from an underestimation of the volume change (which enters the free energy through the pV term) across the transition. For CaO the experimental volume change at the transition pressure is about -10%, whereas VIB predicts a volume change of only -6.3% at this same pressure. For SrO the experimental ΔV is -13% at the transition pressure compared to the VIB prediction of -6.5%. Because phase stability is determined by the (small) difference between two large numbers (the Gibbs free energies of the competing phases),

TABLE I. Structure and elastic properties of MgO, CaO, and SrO at $T = 300$ K. R_e is the zero-pressure nearest-neighbor distance (in angstroms), and K_T is the isothermal bulk modulus (in GPa). The experimental elastic constants are adiabatic values (in GPa), while the calculated elastic constants are "athermal" values, as discussed in the text. The binding energy is given by $\Phi_0 + E_{\rm th}$ (in atomic units) for the equilibrium structure at 300 K.

MgO ($B1$)	R_e	K_T	$\frac{dK_T}{dP}$	C_{11}	C_{12}	C_{44}	$C_{11}-C_{12}$	$C_{44}-C_{12}$	D_e
Expt.[a]	2.106	160	4.1	297	95	156	202	61	1.16[c]
VIB	2.111	160	4.0	278	100	200	178	100	1.17
Rigid ion[b]	2.111	252	4.3	370	194	200	178	6	1.17
CaO ($B1$)	R_e	K_T	$\frac{dK_T}{dP}$	C_{11}	C_{12}	C_{44}	$C_{11}-C_{12}$	$C_{44}-C_{12}$	D_e
Expt.[a]	2.415	111	4.2	221	57	80	164	23	1.01[d]
VIB	2.370	114	4.1	204	69	112	136	43	1.06
Rigid ion[b]	2.370	153	4.3	243	109	112	136	3	1.06
SrO ($B1$)	R_e	K_T	$\frac{dK_T}{dP}$	C_{11}	C_{12}	C_{44}	$C_{11}-C_{12}$	$C_{44}-C_{12}$	D_e
Expt.[a]	2.580	91	4.3	174	47	56	127	9	0.94[d]
VIB	2.534	90	4.2	172	49	83	124	34	0.99
Rigid ion[b]	2.534	122	4.4	204	81	83	124	2	0.99

[a]Experimental values quoted in Ref. 18; see references therein.

[b]"Rigid ion" means the breathing parameters are frozen in at their VIB equilibrium values; hence, R_e is the same as for VIB. The Cauchy condition $C_{44}-C_{12}=0$ is slightly violated here since the volume of the lattice is slightly expanded from the static lattice equilibrium value.

[c]Zero-temperature value quoted in Ref. 18.

[d]300-K value quoted in Ref. 18.

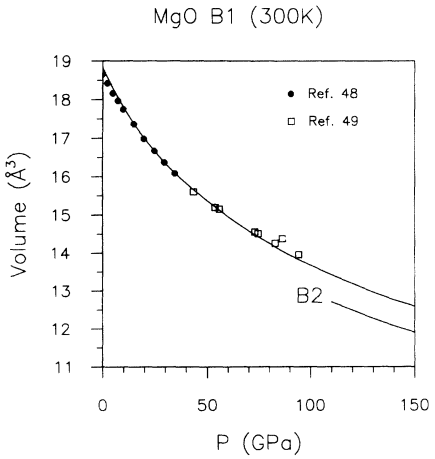

FIG. 2. Calculated equation of state for MgO at 300 K. The experimental points were taken from Refs. 48 and 49.

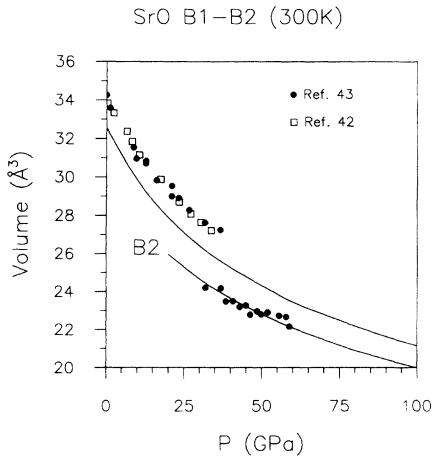

FIG. 4. Calculated equation of state for SrO at 300 K. The experimental points were taken from Refs. 42 and 43.

such seemingly small discrepancies as those present for the CaO and SrO $B1$ volumes can lead to large errors in a model's predictions for transition pressures and temperatures.

The theoretical values for the elastic constants given in Table I were calculated from the harmonic sound velocities derived from the dynamical matrix and are thus neither isothermal nor adiabatic, but are what may be called "athermal;" i.e., the only thermal correction to the static lattice elastic constants is the effect of the quasiharmonic thermal expansion of the lattice. At 300 K, however, the thermodynamic corrections between the adiabatic and athermal elastic constants are very small and can be safely ignored at the present level of accuracy. As shown in Table I, the calculated values for C_{11} and C_{12} are in surprisingly good agreement with the data (within 10%), especially when compared to those obtained from the rigid-ion model. The elastic constant C_{44}, however, is in much poorer agreement with data, typically within 30%. Furthermore, there is no difference between the value of C_{44} calculated using the VIB model and that calculated using the simpler rigid-ion potential. This lack of coupling between C_{44} and spherical breathing is expected from symmetry arguments. C_{44} is a pure shear modulus, and thus no volume change accompanies the strain associated with this modulus. This is also the case for the combination C_{11}-C_{12}, which is also a pure shear modulus; hence, the same calculated values for this modulus are obtained from both the VIB and rigid-ion models.

Because of the coupling of spherical breathing to the elastic deformations associated with C_{12}, the VIB model does allow a relaxation of the Cauchy restriction $C_{12}=C_{44}$ which must be obeyed at zero pressure for all cubic crystals (in their static state) where the atoms interact via central pair potentials alone. Since the VIB model incorporates the first-order many-body effects arising from charge overlap, the Cauchy restriction is violated. In Table I we compare the calculated deviation of the Cauchy relation for these oxides using the VIB and rigid-ion models with the corresponding measured values. Both the sign and magnitude of the deviation obtained from the VIB calculation are in qualitative agreement with the data. In all cases the calculated deviation is larger than observed. This again reflects the fact that C_{44} cannot couple to spherical breathing and is overestimated in the VIB calculation. The table also reveals a slight deviation of the Cauchy relation for the rigid-ion model. This arises from the fact that at 300 K the volume of the lattice is slightly expanded from the equilibrium static lattice value.

To further improve the calculated elastic constants, it will be necessary to include nonspherical deformation of the ionic charge densities. Most importantly, inclusion of quadrupolar deformations will be necessary to reduce C_{44} and further reduce C_{12}.

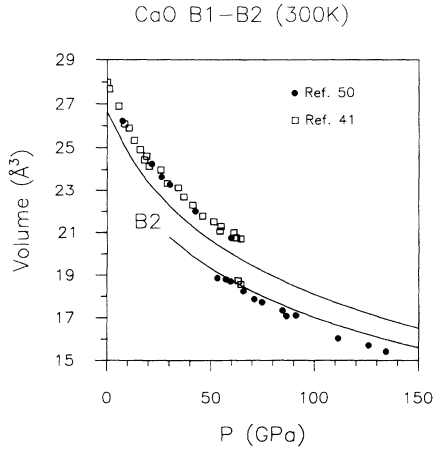

FIG. 3. Calculated equation of state for CaO at 300 K. The experimental points were taken from Refs. 50 and 41.

B. Lattice dynamics

In Figs. 5, 6, and 7 the theoretical dispersion relations of the VIB model are compared to inelastic neutron-scattering data and to the dispersion relations that result when the breathing parameters are frozen in at their

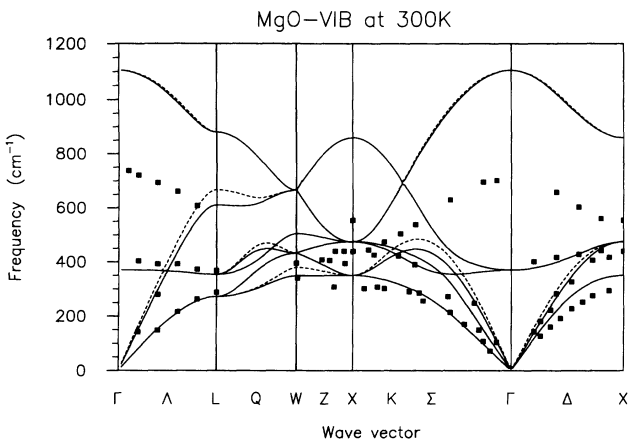

FIG. 5. Calculated phonon dispersion for MgO at 300 K. The solid line represents the VIB result, while the dashed line was obtained from a rigid-ion calculation. The neutron-scattering data, represented by squares, were taken from Ref. 51.

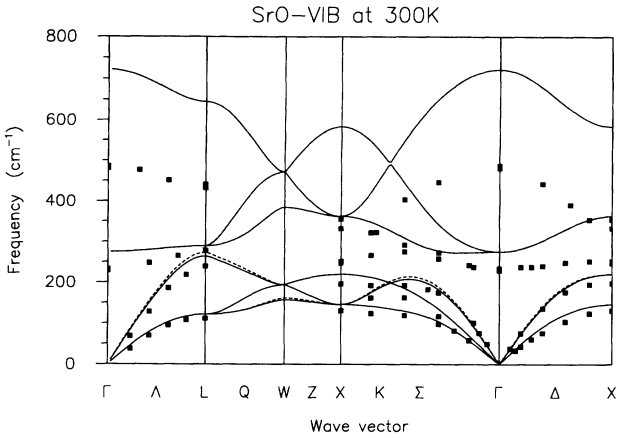

FIG. 7. Calculated phonon dispersion for SrO at 300 K. The solid line represents the VIB result, while the dashed line was obtained from a rigid-ion calculation. The neutron-scattering data, represented by squares, were taken from Ref. 51.

equilibrium values in the VIB model. The agreement between the theoretical acoustic branches and the data is reasonably good for the oxides, reflecting the respective agreement in the elastic constants, which are, after all, linearly related to the squared sound velocities. However, the optic branches, in particular the LO branches, show a much larger deviation from the neutron-scattering data. This discrepancy primarily arises from the neglect of nonspherical breathing in the present VIB treatment.

The most important charge relaxation mechanism affecting the optical branch and the LO-TO splitting is dipolar deformation (polarization). This is because dipolar charge distributions directly couple to the local macroscopic field produced by the ionic motions. Higher-order charge relaxation will have a lesser effect since it only couples to electric field gradients (inhomogeneous electric fields). Moreover, spherically symmetric charge relaxation does not produce any multipole moments, and as a consequence, its coupling to the electric field is even weaker.

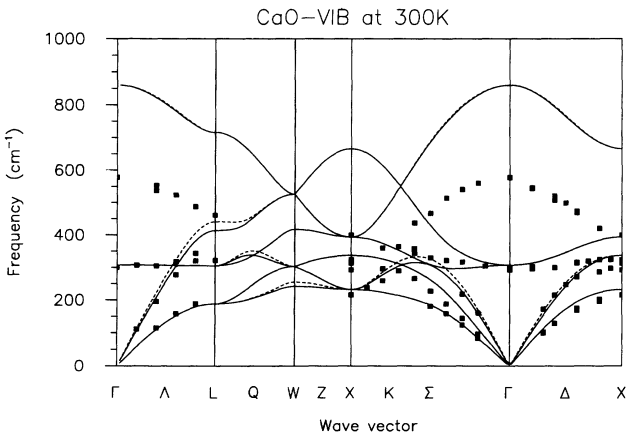

FIG. 6. Calculated phonon dispersion for CaO at 300 K. The solid line represents the VIB result, while the dashed line was obtained from a rigid-ion calculation. The neutron-scattering data, represented by squares, were taken from Ref. 51.

In the PIB model there is a large effect on the LO-TO splitting due to the spherical breathing. However, variations in the long-ranged electrostatic interactions due to the lattice vibrations cannot "induce" spherical breathing unless there is a direct overlap of the "inducing" charge density with the breathing ion, no matter how strong or nonuniform the electric fields. Since the non-Coulombic contributions to the ionic interactions are short ranged,[44] this straightforward argument shows why ionic breathing parameters should *not* couple to the point–Coulomb-site potential. This would appear to contradict the premise on which PIB lattice dynamics is based.

In the plots we also show the corresponding rigid-ion dispersion curves for comparison. It is striking how small the VIB effect is on the optical vibrational frequencies. In the high-symmetry directions, most of the phonon branches show no change in frequency because symmetry prevents the modes from coupling to spherical breathing of the oxygen ions. As expected, the LO-TO splitting of the rigid-ion and VIB models is the same.

To demonstrate the model's usefulness in the calculation of thermal properties, we have used VIB lattice dynamics to determine the temperature dependence of the isothermal and adiabatic bulk moduli of MgO at ambient pressure. For this plot, the isothermal bulk moduli K_T were obtained by fitting the $p(V)$ isotherms to a Birch-Murgnahan equation of state.[45] The adiabatic bulk moduli were obtained from the isothermal value through the thermodynamic identity

$$K_S = K_T \left[1 + \frac{TV\alpha^2 K_T}{C_V} \right], \tag{30}$$

where α is the volume thermal expansivity and C_V is the isochoric heat capacity. To extract the temperature-dependent α, we employed a Mie-Gruneisen fit[46] to the calculated values of V along the ambient pressure isobar. The temperature-dependent C_V values were obtained

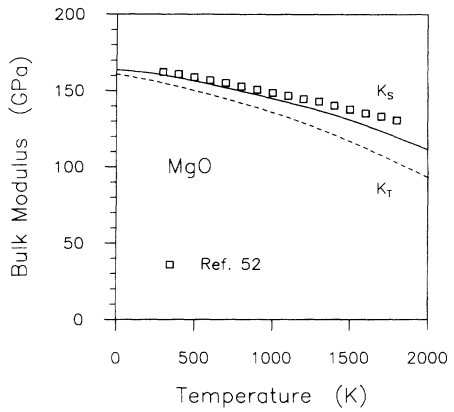

FIG. 8. Isothermal and adiabatic bulk moduli as a function of temperature for MgO. Data taken from Ref. 52.

from the quasiharmonic vibrational density of states in the usual way. The results are shown in Fig. 8 and compare favorably with experimental values. The quasiharmonic predictions for the bulk moduli are only a few percent high throughout the temperature range for which data are available (up to 1800 K).

C. Beyond the Watson sphere

Because the breathing parameters in the VIB model are determined variationally, it is important to work with variational parameters that make the charge density flexible enough so it can relax close to the true ground state. Since the conventional choice of a single breathing parameter (i.e., a variable Watson radius R_w with a fixed charge Q_w chosen to neutralize the ionic charge) might not provide the optimal flexibility, we investigated the effect of additional degrees of freedom for the crystal-charge density (subject to the constraint of spherically symmetric ions) on the calculated ground-state energy, lattice constant, and bulk modulus of MgO and CaO. In the subsequent discussion we investigate, in turn, the importance of four effects: (i) incorporating the Watson charge Q_w as an additional variational parameter, (ii) variability associated with the use of different forms for the confining potential, (iii) the effects due to cation breathing, and (iv) the effect of charge transfer between anions and cations.

We first reexamined the Watson-sphere potential. Introducing Q_w as a second variational parameter lowered the energy of MgO by 5 mRy and decreased the zero-pressure volume by 2% from their corresponding values with Q_w frozen to +2.0. The optimal value for Q_w is slightly pressure dependent and also depends on the countercation. It is interesting that the variational value of Q_w for MgO is $+3.3e$ at zero pressure, considerably larger than the conventional choice of $+2.0e$. The larger value for Q_w can be explained by recalling that in the VIB model the Watson potential simulates the effective crystal potential due to overlapping charge densities.[10] Fixing Q_w at $+2.0e$ leads to an equilibrium Watson radius of 1.16 Å for MgO, which is well inside the O^{2-} ion, whereas relaxing both R_w and Q_w results in a larger Watson charge at a radius of 1.33 Å, which is very close to the classical ionic radius of 1.40 Å for the O^{2-} pseudo-ion.[47] At this distance from the oxygen nucleus, the magnesium-charge density rises steeply and is more realistically simulated by a Watson sphere with this radius and a large charge.

A completely different situation is found in the case of CaO and SrO. In the case of CaO a minimum in the total crystal energy could not be found with respect to variations in *both* R_w and Q_w at zero pressure. To investigate the origin of this instability, we carried out a series of calculations (at $P=0$) in which the Q_w parameter was systematically fixed at different values while the R_w was allowed to vary. The crystal energy gradually decreases as Q_w is reduced from $+2.0e$ with a slight expansion of the lattice in the direction of the measured experimental value. For Q_w values less than about $+1.2e$, O^{2-} was found to be unstable. This may suggest that the ionic description for CaO may be tenuous at zero pressure. At slight positive pressures for CaO, the O^{2-} could be stabilized with both the R_w and Q_w variables. It is interesting to note that the use of self-interaction-corrected (SIC) Kohn-Sham densities led to a larger stability window and stable minimum at $P=0$ with $R_w=1.28$ Å and $Q_w=+1.8e$. Unfortunately, we generally find that the zero-pressure volumes obtained using SIC densities are substantially reduced (4–6%) relative to those obtained from the KS-LDA treatment and in poorer agreement with data. Investigations aimed at understanding the differences introduced by using KS vs SIC-KS densities are currently in progress.

We next examined the effect of using different functional forms for the confining potentials. In our earlier discussion we pointed out that the Watson sphere is only one possible ansatz for an ELMBP. A form for the ELMBP similar to the self-consistent potentials calculated by Zhang and Bukowinski[18] in their MPIB work can be obtained by considering the spherical average of a screened electrostatic potential of the form

$$\phi(r)=-Q_w\frac{e^{-\sigma r}}{r}\ . \tag{31}$$

The spherical average of this potential about a displaced center at $r=R_w$ is then given by

$$W(r)=-Q_w\frac{e^{-\sigma R_w}}{R_w}\tilde{j}_0(\sigma r),\quad r<R_w$$

$$=-Q_w\frac{e^{-\sigma r}}{r}\tilde{j}_0(\sigma R_w),\quad r\geq R_w\ , \tag{32}$$

where $\tilde{j}_0(x)$ is the zeroth-order spherical Bessel function with pure imaginary argument, i.e., $\tilde{j}_0(x)=\sinh x/x$. In the limit $\sigma=0$ this potential reduces to the Watson-sphere potential. An even more elaborate parametrization which mimics certain aspects of the Watson sphere potential, but provides control over the stiffness of the well wall, can be written as

$$W(r)=-\frac{Q_w}{R_w}\left[\frac{1+C^2}{1+(C-y)^2}\right]^{\sigma} e^{-\sigma y/C}, \quad y=(r/R_w)^2 . \tag{33}$$

As $r\to 0$, this potential goes to $-Q_w/R_w$, while asymptotically it behaves as $\simeq r^{-4\sigma}e^{-ar^2}$ with the exponent given by $a=\sigma/(R_w^2 C)$.

Figure 9 illustrates the radial dependence all three of the potentials considered. To simplify the comparison, Q_w has been fixed at $+2.0e$ and all others parameters have been set to their optimal variational values for CaO in the static $B1$ structure. As can be seen from the plots, the difference in the radial dependence of the various potentials is quite dramatic, particularly at high pressure. In spite of this the calculated properties are found to be essentially the same in all three cases. In Table II we list the potential parameters and some calculated crystal properties at the two pressures corresponding to the plots in Fig. 9. The static lattice bulk moduli and the equilibrium zero-pressure lattice constants are seen to be nearly identical in all three cases. Larger discrepancies are found in the crystal properties at ambient pressure compared to those obtained for the higher pressure. On the other hand, there appears to be a larger variability in the radial dependence of the three potentials at high pressure. Similar trends are found in the case of MgO. A remarkable conclusion that emerges from these test calculations is that the crystal properties are relatively insensitive to the precise form of the ELMBP. This would seem to suggest that the simplest Watson-sphere ELMBP ansatz for spherical breathing (with a fixed Q_w and variable R_w) is adequate.

It is also of interest to determine the importance of cation breathing. Introducing an additional Watson sphere around the Ca^{2+} ion in CaO and relaxing the static lattice energy with respect to both Watson radii and the cation Q_w reduced the energy per unit cell by only 0.3 mRy and resulted in a lattice volume that was contracted by 0.2% compared to the rigid-cation result. The effect is even smaller in MgO because Mg^{2+} is less deformable than the larger Ca^{2+} ion. We therefore conclude that, compared to oxygen breathing, spherical charge relaxation of the cations is of relatively minor importance.

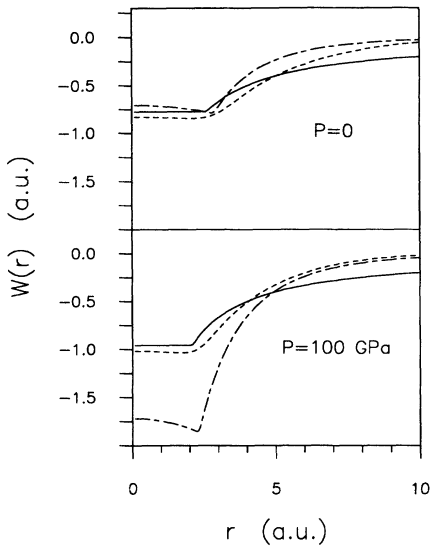

FIG. 9. Optimal ELMBP for static lattice CaO ($B1$) at 0 and 100 GPa. The solid lines represent the results obtained by optimizing the Watson-sphere potential with respect to both R_w. The dashed and dot-dashed curves denote the optimal potentials given by Eqs. (33) and (32), respectively.

It is interesting to note that the variationally-optimized Watson charge for the cation is positive and thus has the opposite sign of the charge that would be assigned to a cation in a PIB-type treatment, where Q_w is chosen to neutralize the ionic charge. This observation is consistent with the notion that overlap repulsion determines ionic sizes in crystals rather than the electrostatic site potential.

The last issue we shall address in connection with the modeling of oxide crystals is the adequacy of the closed-shell description itself. We have investigated this ques-

TABLE II. Optimal variational parameters for three choices of the confining potential for CaO at zero pressure. The potentials WR2 and WR are, respectively, Watson-sphere potentials with and without the variable Q_w. The bulk moduli (in units of GPa) were evaluated for a static lattice. Volume in Å^3 and lengths in Å.

Potential	R_w	Q_w	C	σ	K_T	R_e	Φ_0
$P=0$ GPa							
WS	2.591	2.000			119	2.361	−1.432 37
Eq. (33)	2.848	2.000	0.151	1.25	120	2.363	−1.429 85
Eq. (32)	2.412	2.000		0.30	121	2.357	−1.423 55
$P=100$ GPa							
WS	2.087	2.000				2.080	−0.950 59
WS2	2.020	1.822				2.080	−0.950 76
Eq. (33)	1.964	2.000	0.151	1.25		2.081	−0.946 31
Eq. (32)	2.328	2.000		0.30		2.079	−0.941 75

tion within the context of a spherical-ion model by allowing for fractional charge transfer between the anions and cations. In order to treat these effects, the KS numerical procedure was modified to allow fractional occupation numbers. Special care was taken to ensure the continuity of "single-particle" and total energies across shell boundaries. The VIB and MEG procedures were then modified to treat the fractional charge δQ as an additional variational parameter. The latter quantity is defined as the additional fractional charge on an anion. Thus a negative value of δQ represents the removal of charge from a closed anion p shell and its addition to an open s shell of a cation. Within the framework of our simplified computational scheme, this is the simplest nontrivial way to achieve a measure of the effects of charge transfer.

It should be emphasized that the coupling between the ionic breathing and the charge transfer is provided by the VIB procedure. In the most general case, the free energy of the crystal is minimized with respect to the breathing parameters R_w and Q_w and the fractional charge parameter δQ. For all the cubic oxides considered, we find that the variationally-optimized ionic charges are within less than 1% of the corresponding formal values.

Very recently, Illas *et al.*[33] performed a study to determine the character of bonding in the alkaline earth oxides. Specifically, they performed a series of calculations based on cluster-model determinantal wave functions of increasing complexity and compared their results with the predictions of full configuration interaction (CI) calculations. They find that the ideal ionic configuration (e.g., corresponding to a superposition of closed-shell ionic densities) has a weight of more than 95% in the final CI wave function. In addition, the ionic charge states of the ions in the crystal deviated from their formal ionic values of $\pm 2e$ by no more than a few percent. This latter observation is consistent with our findings. Finally, from an analysis of the CI wave functions, Illas *et al.* determined that electron-electron correlation effects were mainly intra-atomic. Our electron-gas calculations also reveal that the inclusion of LDA correlation energy in the GK formula tends to contract the lattice and worsen the agreement with the experimental equations of state. Our work also indicates that the inclusion of correlation energy in the KS description of the individual ions leads to a more realistic description of the crystal properties.

Within the context of our model, this tendency toward closed-shell character can be understood in terms of the substantial energy cost associated with the fractional charge transfer between ions. For positive δQ there is a strong decrease in repulsion which is compensated by an equally large increase in the Madelung energy and self-energy. Overall, we find that this approximate treatment of charge transfer in our model has no effect on the calculated properties.

V. CONCLUSIONS

In this paper we studied the influence of ionic breathing on the statics and dynamics of the binary alkaline earth oxides by treating the structural and electronic degrees of freedom variationally. We have shown that a description of the crystal energetics based on a simplified density-functional approach is able to quantitatively reproduce most of the observed thermoelastic properties of these oxides.

Our work confirms the notion that spherical breathing is an important relaxation mechanism in these systems. We find that variational optimization of this effect (VIB) leads to a significant improvement over the conventional rigid-ion description.

We tested the sensitivity of our model to different functional forms for the effective many-body potentials and found that the essential physics is captured by a single variational parameter on the anion. We find that the arbitrariness in the choice of the breathing potential does not appear to affect the predictions of our basic model.

Our calculated equations of state for the $B1$ phase of MgO and the $B2$ phases of CaO and SrO are in excellent agreement with available experimental data. The overestimation of the transition pressures for CaO and SrO seems to be related to the slight underestimation of the $B1$ volumes near the observed transition pressure in both cases. The accuracy of the VIB-model predictions is found to be on the order of a few percent for the lattice constants and bulk moduli. We do not expect that significant improvement on this degree of accuracy is possible within the simplified electron-gas description on which our model is based. Since the influence of using different correction schemes for the energy functionals on the electron-gas results is of about this order of magnitude, it is at this point difficult to unambiguously decide from the degree of agreement with experiment (and more accurate first-principles calculations) which of several alternate electron-gas energy functionals is to be preferred in this type of model.

We also formulated a lattice dynamics description based on VIB in which the breathing (electronic) parameters are treated as dynamical variables. With no adjustable parameters we find that our model provides a very good description of the elastic properties of MgO, CaO, and SrO. In particular, the Cauchy relation predicted by our VIB treatment for these systems is of the correct sign, although the magnitude of the difference $C_{44}-C_{12}$ is somewhat larger than its experimental counterpart. We expect that the introduction of nonspherical deformations will greatly reduce these and other related discrepancies with experiment. In particular, taking quadrupolar deformations into account seems necessary to improve the predictions for the elastic constants, while a model for dipolar charge relaxation is required to eliminate the overestimation of the optical vibrational frequencies.

The simplicity of the VIB model together with its predictive character encourage the use of the approach (and in the future possibly extended versions that include nonspherical charge relaxation) in theoretical studies of even more comples ionic materials which are currently beyond the computational reach of more elaborate and sophisticated *ab initio* techniques.

ACKNOWLEDGMENTS

The Materials Research Group at Arizona State University generously provided us access to their computa-

tional resources. Andrew Chizmeshya is supported by the Associated Western Universities. This work was supported through the EG&G Idaho Long-Term Research Initiative under DOE Idaho Operations Office Contract No. DE-AC07-76IDO1570 and by National Science Foundation Grant No. EAR-9105510.

APPENDIX

Here we provide explicit expressions for the dynamical matrix elements. Our notation is as follows: $\mathbf{R}(^{l}_{\nu})$ denotes the position of the νth ion in the lth primitive unit cell. Similarly, $\zeta(^{l}_{\nu})$ represents the ELMBP variational parameters. We discuss here only the contributions to the dynamical matrix from Φ, the short-ranged overlap part of the interaction, and Φ^{s}, the self-energy piece. Since the Coulomb contributions do not involve the breathing parameters and can be treated using conventional methods,[37] we do not present detailed formulas for them here.

$$\mathcal{D}_{ij}^{RR}(\nu\nu'|\mathbf{q})=\left[\frac{1}{m_\nu m_{\nu'}}\right]^{1/2}\sum_{l\neq 0}\left[-\frac{R_iR_j}{R^2}\left[\Phi''(^{l\ 0}_{\nu\ \nu'})-\frac{\Phi'(^{l\ 0}_{\nu\ \nu'})}{R}\right]-\delta_{ij}\frac{\Phi'(^{l\ 0}_{\nu\ \nu'})}{R}\right]e^{i\mathbf{q}\cdot\mathbf{R}(l)}$$
$$+\delta_{\nu\nu'}\frac{1}{m_\nu}\sum_{m\neq 0}\sum_{\mu}\left[\frac{R_iR_j}{R^2}\left[\Phi''(^{m\ 0}_{\mu\ \nu})-\frac{\Phi'(^{m\ 0}_{\mu\ \nu})}{R}\right]+\delta_{ij}\frac{\Phi'(^{m\ 0}_{\mu\ \nu})}{R}\right]. \tag{A1}$$

In this formula $\mathbf{R}(l)\equiv\mathbf{R}(^{l}_{\nu})-\mathbf{R}(^{0}_{\nu})$, $R^2\equiv\mathbf{R}(l)\cdot\mathbf{R}(l)$, and $\Phi(^{l\ l'}_{\nu\ \nu'})$ is the pair potential between ions $(^{l}_{\nu})$ and $(^{l'}_{\nu'})$. The primes on the potentials in matrix elements above denote radial derivatives, and i and j are Cartesian indices.

The mixed $R\zeta$ matrix elements take the form

$$\mathcal{D}_{i}^{R\zeta}(\nu\nu'|\mathbf{q})=\left[\frac{1}{m_\nu}\right]^{1/2}\sum_{l\neq 0}\left[-\frac{R_i}{R}\frac{\partial^2\Phi(^{l\ 0}_{\nu'\ \nu})}{\partial R\,\partial\zeta(^{l}_{\nu'})}\right]e^{i\mathbf{q}\cdot\mathbf{R}(l)}+\delta_{\nu\nu'}\left[\frac{1}{m_\nu}\right]^{1/2}\sum_{m\neq 0}\sum_{\mu}\left[-\frac{R_i}{R}\frac{\partial^2\Phi(^{m\ 0}_{\mu\ \nu})}{\partial\zeta(^{0}_{\nu})\partial R}\right] \tag{A2}$$

and

$$\mathcal{D}_{j}^{\zeta R}(\nu\nu'|\mathbf{q})=\left[\frac{1}{m_\nu}\right]^{1/2}\sum_{l\neq 0}\left[\frac{R_j}{R}\frac{\partial^2\Phi(^{l\ 0}_{\nu'\ \nu})}{\partial R\,\partial\zeta(^{0}_{\nu})}\right]e^{i\mathbf{q}\cdot\mathbf{R}(l)}+\delta_{\nu\nu'}\left[\frac{1}{m_\nu}\right]^{1/2}\sum_{m\neq 0}\sum_{\mu}\left[-\frac{R_j}{R}\frac{\partial^2\Phi(^{m\ 0}_{\mu\ \nu})}{\partial\zeta(^{0}_{\nu})\partial R}\right], \tag{A3}$$

while the pure VIB matrix elements are expressible in the form

$$\mathcal{D}^{\zeta\zeta}(\nu\nu'|\mathbf{q})=\sum_{l\neq 0}\frac{\partial^2\Phi(^{l\ 0}_{\nu'\ \nu})}{\partial\zeta(^{0}_{\nu})\partial\zeta(^{l}_{\nu'})}e^{i\mathbf{q}\cdot\mathbf{R}(l)}+\delta_{\nu\nu'}\sum_{m\neq 0}\sum_{\mu}\frac{\partial^2\Phi(^{m\ 0}_{\mu\ \nu})}{\partial\zeta(^{0}_{\nu})\partial\zeta(^{0}_{\nu})}+\delta_{\nu\nu'}\frac{\partial^2\Phi^{s}}{\partial\zeta(^{0}_{\nu})\partial\zeta(^{0}_{\nu})}. \tag{A4}$$

[1]R. G. Gordon and R. LeSar, Adv. Quantum Chem. **21**, 341 (1990).
[2]W. Kohn and L. J. Sham, Phys. Rev. **140**, A1133 (1965).
[3]R. G. Gordon and Y. S. Kim, J. Chem. Phys. **56**, 3122 (1972).
[4]M. J. Clugston, Adv. Phys. **27**, 893 (1978).
[5]Y. S. Kim and R. G. Gordon, Phys. Rev. B **9**, 3548 (1974).
[6]A. J. Cohen and R. G. Gordon, Phys. Rev. **12**, 3228 (1975).
[7]L. L. Boyer, Phys. Rev. Lett. **45**, 1858 (1980); L. L. Boyer, Phys. Rev. B **23**, 3673 (1981).
[8]L. L. Boyer and J. R. Hardy, Phys. Rev. B **24**, 2577 (1981).
[9]L. L. Boyer, J. Phys. C **17**, 1825 (1984).
[10]R. E. Watson, Phys. Rev. **111**, 1108 (1958).
[11]C. Mulhausen and R. G. Gordon, Phys. Rev. B **23**, 900 (1981).
[12]R. J. Hemley and R. G. Gordon, J. Geophys. Res. **90**, 7803 (1985).
[13]M. J. Mehl, R. J. Hemley, and L. L. Boyer, Phys. Rev. B **33**, 8685 (1976).
[14]A. J. Cohen and R. G. Gordon, Phys. Rev. B **14**, 4593 (1976).
[15]G. H. Wolf and M. S. T. Bukowinski, Geophys. Res. Lett. **12**, 809 (1985).
[16]G. H. Wolf and M. S. T. Bukowinski, in *US-Japan Joint Seminar on High Pressure Research: Applications in Geophysics and Geochemistry*, edited by M. Manghnanai and S. Akimoto (Kluwer Academic, Norwell, MA, 1987).
[17]G. H. Wolf and M. S. T. Bukowinski, Phys. Chem. Miner. **15**, 209 (1988).
[18]H. Zhang and M. S. T. Bukowinski, Phys. Rev. B **44**, 2495 (1991).
[19]A. N. Basu and S. Sengupta, Phys. Status Solidi B **102**, 117 (1980).
[20]M. D. Jackson and R. G. Gordon, Phys. Chem. Miner. **16**, 212 (1988).
[21]D. L. Lacks and R. G. Gordon, Phys. Rev. B **48**, 2889 (1993).
[22]D. L. Lacks and R. G. Gordon, J. Geophys. Res. **98**, 22 147 (1993).
[23]R. E. Cohen, L. L. Boyer, and M. J. Mehl, Phys. Rev. B **35**, 5749 (1987).
[24]P. Hohenberg and W. Kohn, Phys. Rev. **136**, 864 (1964).
[25]O. Gunnarsson and B. I. Lundqvist, Phys. Rev. B **13**, 4274 (1976).
[26]J. Harris, Phys. Rev. B **31**, 1770 (1985).
[27]C. C. Shih, Mol. Phys. **38**, 1225 (1979).
[28]K. Yonei and Y. Tomishima, J. Phys. Soc. Jpn. **20**, 1051 (1965).

[29]Y. Tomishima and K. Yonei, J. Phys. Soc. Jpn. **21**, 142 (1966).
[30]W. Stich, E. K. Gross, P. Malzacher, and R. M. Dreizler, Z. Phys. A **209**, 5 (1982).
[31]E. W. Pearson and R. G. Gordon, J. Chem. Phys. **82**, 881 (1985).
[32]D. L. Lacks and R. G. Gordon, J. Chem. Phys. **100**, 4446 (1994).
[33]F. Illas, A. Lorda, J. Rubio, J. B. Torrence, and P. S. Bagus, J. Chem. Phys. **99**, 389 (1993).
[34]P. P. Ewald, Ann. Phys. (Leipzig) **64**, 253 (1921).
[35]B. G. Dick and A. W. Overhauser, Phys. Rev. **112**, 90 (1958).
[36]U. Schroder, Solid State Commun. **4**, 347 (1966).
[37]A. A. Maradudin, E. W. Montroll, G. H. Weiss, and I. P. Ipatova, *Theory of Lattice Dynamics in the Harmonic Approximation,* 2nd ed. (Academic, New York, 1971).
[38]D. C. Wallace, *Thermodynamics of Crystals* (Wiley, New York, 1972).
[39]W. H. Press, B. P. Flannery, S. A. Teukolsky, and W. T. Vetterling, *Numerical Recipes* (Cambridge University Press, New York, 1986).
[40]B. Svendesen and T. J. Ahrens, Geophys. J. R. Astron. Soc. **91**, 667 (1987).
[41]J. F. Mammone, M. K. Mao, and P. M. Bell, J. Phys. Geophys. Res. Lett. **8**, 140 (1981).
[42]Y. Sato and R. Jeanloz, J. Geophys. Res. **86**, 11 773 (1981).
[43]L. G. Liu and W. Bassett, J. Geophys. Res. **78**, 8470 (1973).
[44]This argument can still be applied to the LO-TO splitting even if longer-ranged electron correlation forces are included (going beyond the local-density approximation for the correlation energy). They will still fail to provide coupling to a macroscopic electric field as long as a spherically symmetric charge distribution is retained.
[45]F. Birch, J. Geophys. Res. **83**, 1257 (1978).
[46]I. Suzuki, J. Phys. Earth **23**, 145 (1975).
[47]N. W. Ashcroft and N. D. Mermin, *Solid State Physics* (Holt, Reinhart and Winston, Philadelphia, 1976).
[48]E. Perez-Albuerne and H. Drickamer, J. Chem. Phys. **43**, 1381 (1965).
[49]M. K. Mao and P. M. Bell, J. Geophys. Res. **84**, 4533 (1979).
[50]P. Richet, M. K. Mao, and P. M. Bell, J. Geophys. Res. Lett. **80**, 15 279 (1988).
[51]H. Bilz and W. Kress, *Phonon-Dispersion Relations in Insulators,* Springer Series in Solid State Sciences Vol. 10 (Springer-Verlag, Berlin, 1979).
[52]D. G. Isaak, R. E. Cohen, and M. J. Mehl, J. Geophys. Res. **95**, 7055 (1990).